Available online at www.sciencedirect.com
ScienceDirect
Journal of the European Ceramic Society 30 (2010) 1401–1408
www.elsevier.com/locate/jeurceramsoc

Hot-corrosion behaviors of overlay-clad yttria-stabilized zirconia coatings in contact with vanadate–sulfate salts

X.H. Zhong [a,b], Y.M. Wang [c], Z.H. Xu [a,b], Y.F. Zhang [a,b], J.F. Zhang [a,b], X.Q. Cao [a,*]

[a] State Key Laboratory of Rare Earth Resources Utilization, Changchun Institute of Applied Chemistry, Chinese Academy of Sciences, Changchun 130022, China
[b] Graduate School of the Chinese Academy of Sciences, Beijing 100049, China
[c] Jilin Province Laser Institute, Changchun 130012, China

Received 20 April 2009; received in revised form 8 October 2009; accepted 22 October 2009
Available online 8 December 2009

Abstract

A dense clad overlay with chemical inertness was achieved on top of the plasma-sprayed YSZ thermal barrier coatings by laser in order to protect them from hot-corrosion attack. The Al_2O_3-clad YSZ coating exhibited good hot-corrosion behavior in contact with salt mixture of vanadium pentoxide (V_2O_5) and sodium sulfate (Na_2SO_4) for a longtime of 100 h at 1173 K. The $LaPO_4$-clad YSZ coating showed corrosion resistance inferior to the Al_2O_3-clad one. Yttria was leached from YSZ by reaction between Y_2O_3 and V_2O_5, which caused progressive destabilization transformation of YSZ from tetragonal (*t*) to monoclinic (*m*) phase. The chemical inertness of the clad layers and the restrained infiltration of the molten corrosive salts by the dense clad layers were primary contributions to improvement of the hot-corrosion resistances.

Keywords: Hot corrosion; Laser cladding; Phase transformation; Thermal barrier coatings

1. Introduction

Thermal barrier coatings (TBCs) are widely used in gas turbines to provide insulation for hot sections and also to increase turbine efficiency. Currently, state-of-the-art duplex TBC system comprises the YSZ (zirconia stabilized with 6–8 wt.% yttria) top coat applied over an oxidation-resistant MCrAlY (M = Ni and/or Co) metallic bond coat. Previous results demonstrated that oxidation of bond coat and thermal mismatch between ceramic coating and superalloy substrate were main factors that limit lifetimes of TBCs used in aviation gas turbines.[1–6]

TBCs are also finding increasing application in land-based industrial engines and sea engines that are usually operated in corrosive environments or burn low-quality fuels containing impurities, such as vanadium, sodium, and sulfur. In this case, another failure mode, hot corrosion, becomes predominant and crucial to the lifetimes of TBCs. During long-term service, molten sulfate and vanadate salts condense on the TBCs at the temperature of 600–1000 °C.[7–11] Interconnected pores and microcrack networks in the plasma-sprayed YSZ coatings reduce thermal conductivity and also affect mechanical properties of the coatings. However, these pores and microcracks inevitably provide infiltration paths for molten salts to attack the coatings. Therefore, hot-corrosion resistance over long-term exposures in low-quality fuel combustion or corrosive environments is highly essential for expansive application of TBCs.

In previous studies, a variety of methods have been performed to seal the coating surface, including liquid metal impregnation, hot isostatic press (HIP), laser glazing, sol–gel process, thin chemical vapor deposition (CVD), physical vapor deposition (PVD), plasma-sprayed (PS) and electron beam-physical vapor deposition (EB-PVD) overcoatings, to prevent the penetration of molten salts into the porous YSZ coatings.[12–30] Laser treatment has been proved to be a highly promising method to improve the coating quality of the plasma-sprayed coatings by eliminating open pores within the coating surface and generating a controlled segmented crack network. Hot-corrosion tests in the presence of V_2O_5 indicated that the lifetimes of the plasma-sprayed 6.1YSZ, 7.3YSZ, 12YSZ and 19.5YSZ (numbers denote wt.% of Y_2O_3) coatings were largely increased

* Corresponding author. Tel.: +86 431 85262285; fax: +86 431 85262285.
E-mail address: xcao@ciac.jl.cn (X.Q. Cao).

0955-2219/$ – see front matter © 2009 Elsevier Ltd. All rights reserved.
doi:10.1016/j.jeurceramsoc.2009.10.017

Table 1
Plasma-spraying parameters for the bond coat and the 8YSZ top coat.

Coatings	Current (A)	Voltage (V)	Spraying distance (mm)	Plasma gas (SLM[a])	Carrier gas Ar (SLM)	Powder feed (g min^{-1})	Pressure (kPa)
Bond coat	650	70	250	Ar, 65/H_2, 4	4	30	7.9
8YSZ	900	29	80	Ar, 33/He, 14	5.2	20	–

[a] SLM = standard liter per minute.

after laser glazing.[19,20] Chen et al.[27] reported that Al_2O_3 overlay had been deposited on top of 8YSZ coating by EB-PVD, and Al_2O_3 overlay had refrained structural destabilization of the inner YSZ coating. Afrasiabi et al.[28] demonstrated that PS Al_2O_3 overlay had shown good promise as a potential hot-corrosion barrier for 8YSZ coating. Laser cladding is also an effective method to improve performance of coatings including corrosion resistance.[31–33] Yue et al.[31] reported that laser cladding of composite coating containing Al_2O_3 on aluminum alloy had exhibited good corrosion resistance. Lanthanum phosphate ($LaPO_4$) has good corrosion resistance in environments containing sulfur and vanadium salts.[34,35] However, to our best knowledge, no $LaPO_4$ TBC is reported for composition change of $LaPO_4$ after high-temperature fabrication.

In our former work, the plasma-sprayed 8YSZ coating was laser glazed and achieved remarkably improved hot-corrosion resistance against molten $V_2O_5 + Na_2SO_4$ salts. In the present paper, the 8YSZ coatings were laser-clad with Al_2O_3 and $LaPO_4$, and the hot-corrosion behaviors of the overlay-clad 8YSZ coatings in contact with molten $V_2O_5 + Na_2SO_4$ salts were studied.

2. Experimental

2.1. Specimen preparations

DZ125 nickel-based superalloy with a thickness of 3 mm was chosen as TBC substrate in this study. A bond coat of NiCoCrAlYTa superalloy was deposited on the substrate by low-pressure plasma-spraying (LPPS) using a Sulzer Metco Vacuum Plasma-Spray Unit. The thickness of the bond coat was 100 μm approximately. The substrate was firstly grit-blasted with alumina particles before deposition to increase bond strength between substrate and bond coat. The atmospheric plasma-spraying (APS) of the 8YSZ coating on top of the bond coat was carried out by spraying the 8YSZ powder (204NS, Sulzer Metco) using a Praxair-Tafa 5500-2000 Plasma-Spray unit with a SG-100 plasma-spray gun. Simultaneously, 8YSZ was also directly sprayed on stainless-steel substrate without bond coat. The steel substrate coating was used for characterizations of composition and microstructure before laser cladding. The as-sprayed 8YSZ coating was about 400 μm in thickness. The plasma-spraying parameters for the bond coat and the ceramic top coat are listed in Table 1.

2.2. Feed powder preparations

The $Al(OH)_3$ powder (99.5%, Jinan Jinyingtai Chemicals) was heated at 1673 K for 12 h in order to get α-Al_2O_3. La_2O_3 (99.9%, Guangdong Chenghai Sanxing Chemicals) was dissolved in a diluted phosphoric acid at the molar ratio of La:P = 1:1, and the precipitates were washed several times with de-ionized water until the pH value of the filtered water was close to 7. Then the as-received powder was heated at 1273 K for 2 h in order to obtain pure $LaPO_4$ as a final product. The as-prepared powders of both Al_2O_3 and $LaPO_4$ were spray-dried (GZ-5, Yangguang Ganzao), and the free-flowing spray-dried powders with particle size between 32 μm and 50 μm were collected and used directly as feed powders for laser cladding.

2.3. Laser cladding

Laser cladding of Al_2O_3/$LaPO_4$ on top of the 8YSZ coatings was carried out using an industrial high power (5 kW) continuous-wave CO_2 gas laser (10.6 μm wavelength) with a three-axis CNC workstation. Argon was used as carrier gas for Al_2O_3/$LaPO_4$ feed powders. The laser beam was directed perpendicular to the coating surface during the laser-cladding process. In order to cover the coating surface completely, the samples were subjected to multiple scans with an overlap of 50% between consecutive tracks, always in the same direction. The laser-cladding parameters for the 8YSZ coatings are listed in Table 2.

2.4. Hot-corrosion tests

For comparison, the hot-corrosion tests were performed on the plasma-sprayed, Al_2O_3-clad and $LaPO_4$-clad 8YSZ coatings simultaneously. The coating specimens were sectioned into a dimension of 1 cm × 1 cm. The $V_2O_5 + Na_2SO_4$ mixture

Table 2
Laser-cladding parameters for the 8YSZ coatings.

Laser treatments	Power (W)	[a]Laser beam moving speed (mm min^{-1})	Beam spot (mm^2)	Overlap (mm)	Power density (W mm^{-2})	Powder feed rate (g min^{-1})	Loading gas flux (Ar, SLM)
Claddded Al_2O_3	130	7000	0.8 × 0.8	0.4	203.1	1.5	180
Claddded $LaPO_4$	300	7000	1.5 × 1.5	0.7	133.3	1.3	200

[a] Laser beam moving speed: the moving speed of specimen on the CNC table.

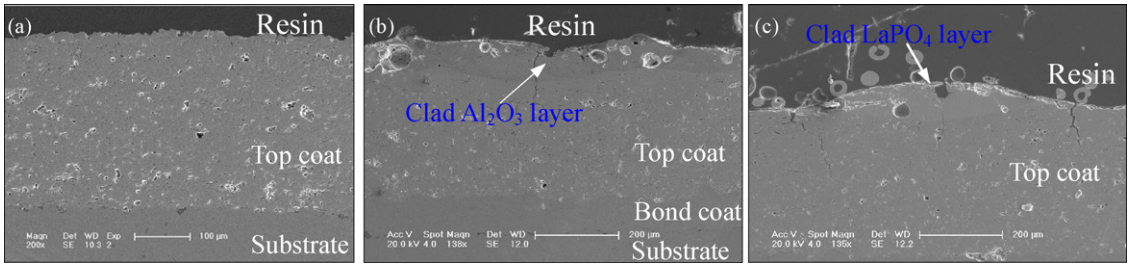

Fig. 1. Cross-sectional microstructures of the 8YSZ coatings: (a) as-sprayed; (b) Al_2O_3-clad; (c) $LaPO_4$-clad, perpendicular to the laser beam moving direction.

(5 mol.%) was applied uniformly over the coatings surface to a coverage of 10 mg cm^{-2}. Then the specimens were isothermally heated at 1173 K in air for 100 h in an electric furnace. Upon heating, the salt mixture was molten on the coating surface. Following a 100-h dwell, the specimens were furnace-cooled down to room temperature.

2.5. Characterizations

The X-ray diffraction (XRD, Rigaku D/Max 2500 diffractometer with Cu-K_α radiation 1.5406 Å) was used for the phase identification and hot-corrosion products. In order to investigate the phase inside the coating, the coating surface was ground until a thin layer of approximately 80 μm was removed before the XRD analysis. The surface morphology and cross-sectional microstructure of the coatings were investigated by scanning electron microscopy (SEM, XL 30 ESEM FEG, Micro FEI Philips), and the elemental distribution was analyzed by means of energy dispersive spectroscopy (EDS). For cross-sectional microstructure analysis, the specimens were embedded in epoxy resin and polished down to 1 μm using diamond paste.

3. Results and discussion

3.1. Characterizations of coatings before and after laser cladding

The cross-sectional microstructures of the 8YSZ coatings before and after laser cladding are exhibited in Fig. 1. It is clearly shown in Fig. 1a that the as-sprayed 8YSZ coating has porous microstructure that is typical microstructure of plasma-sprayed coating. As can be seen from Fig. 1b and *c*, the two overlay-clad 8YSZ coatings both contain an external densified layer. The molten pool solidified rapidly as the laser beam has passed by, giving rise to the elimination of a majority of pores within the coating surface, consequently the dense overlay was induced. The Al_2O_3-clad layer has a thickness of 80–100 μm (Fig. 1b), while that of $LaPO_4$ is 50–100 μm (Fig. 1c). In addition, segmented cracks perpendicular to the coating surface were formed within the densified layers after laser treatments as shown in Fig. 1b and c, which were characteristic features of laser-remelted ceramic materials.[14–22] During laser treatments, the coating surface was molten rapidly and then cooled immediately after the laser beam passed by, and therefore the segmented

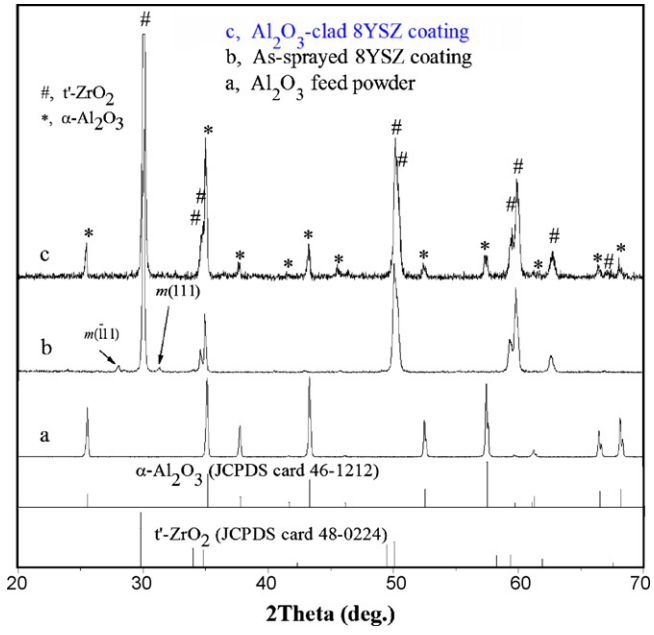

Fig. 2. XRD patterns of the Al_2O_3 feed powder (a); the plasma-sprayed 8YSZ coating (b); Al_2O_3-clad 8YSZ coating (c).

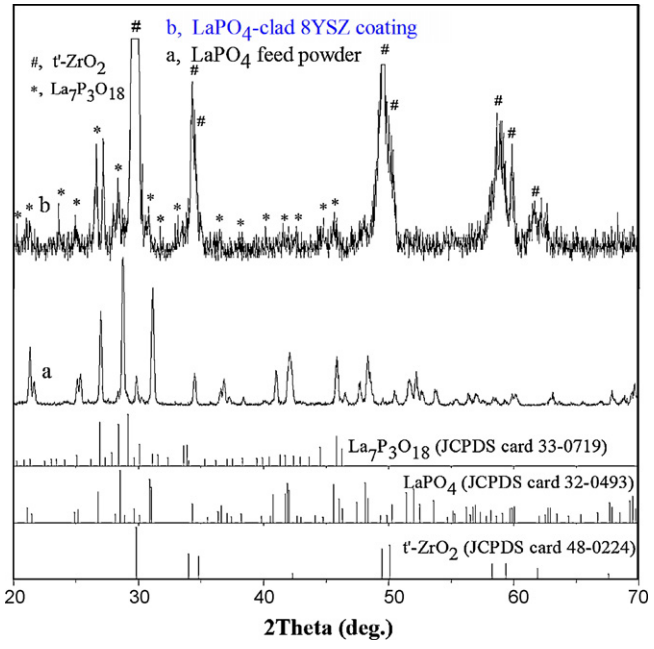

Fig. 3. XRD patterns of the $LaPO_4$ feed powder (a); and the $LaPO_4$-clad 8YSZ coating (b).

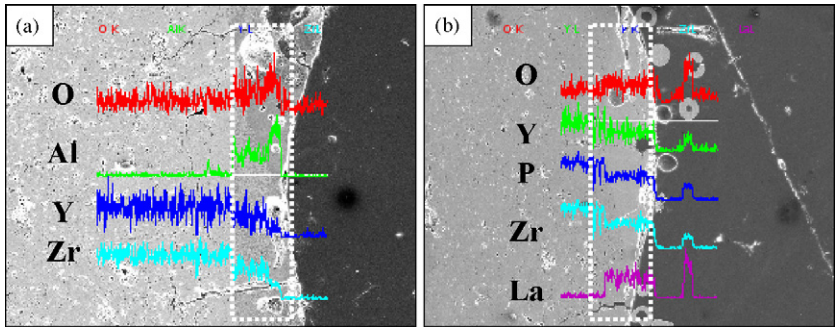

Fig. 4. Cross-sectional micrographs and the corresponding elemental distributions analyzed by EDS for the 8YSZ coatings: (a) Al_2O_3-clad; (b) $LaPO_4$-clad.

cracks were caused by the shrinkage of the molten materials and by the relief of thermal-induced residual stresses during cooling. These segmented cracks perpendicular to the coating surface play an important role in enhancing the thermal-shock resistance by improving the strain accommodation.

The XRD patterns of the as-sprayed and Al_2O_3-clad 8YSZ coating surface are compared in Fig. 2. As shown in Fig. 2b, the as-sprayed 8YSZ coating predominantly crystallizes in non-transformable (t') phase and contains a tiny amount of residual monoclinic (m) phase derived probably from partially molten particles with inhomogeneous composition. It is generally accepted that the rapid solidification of YSZ during plasma-spraying process drives the diffusionless transformation from cubic (c) phase to t'-phase without a composition change. The Al_2O_3-clad 8YSZ coating surface is composed of α-Al_2O_3 and t'-ZrO_2, and m-ZrO_2 is absent (Fig. 2c). The homogenization of chemical composition of t'- and m-phase presented within the as-sprayed 8YSZ coating surface during instant melting and rapid cooling exclusively contributes to the complete formation of t'-ZrO_2. The presence of thermodynamically stable α-Al_2O_3 within the coating surface is a characteristic feature of laser-treated Al_2O_3, which is in agreement with previous investigations.[36–39]

The XRD pattern of the $LaPO_4$-clad 8YSZ coating surface is shown in Fig. 3, together with the data of $LaPO_4$ feed powder. The as-prepared $LaPO_4$ used as feed powder is a pure phase and crystallizes in monazite structure as shown in Fig. 3a. After the laser cladding, $LaPO_4$ transformed to $La_7P_3O_{18}$ as exhibited by Fig. 3b. $LaPO_4$ is a line compound that melts congruently but small deviations from stoichiometry change its solidus temperature from ~2343 K to 1853 K on the La-rich side, or to 1323 K on the P-rich side. Slight deviations in composition could then induce changes in volume and concentration of the molten pool, with resulting variations in evaporation rate and vapor composition.[34] Therefore the rapid melting of $LaPO_4$ during the laser-treatment process resulted in its composition deviation from the stoichiometric $LaPO_4$ and formation of the La-rich compound $La_7P_3O_{18}$.

Fig. 4 exhibits the elemental distributions within the clad layers. As shown in Fig. 4a, the contents of Al and O within the clad layer, as expected, are increased gradually towards the coating surface, while the contents of Y and Zr are decreased (see the dashed square). This result indicates that a eutectic of Al_2O_3 and YSZ is formed after laser cladding, and fractional content of Al_2O_3 within the clad layer is increased gradually towards the coating surface. For the $LaPO_4$-clad 8YSZ coating, as shown in Fig. 4b, the content distributions of Y and Zr within the clad layer were similar to that within the clad Al_2O_3 layer. The contents of La, P and O within the clad layer are increased gradually towards the coating surface. The content of P is not increased so much as that of La, which is attributed to the formation of La-rich compound $La_7P_3O_{18}$.

3.2. Hot-corrosion resistance and failure analysis

The cross-sectional back-scattered electron micrographs (BSE) of the exposed coatings after the hot-corrosion tests are shown in Fig. 5. It is clearly shown in Fig. 5a that serious cracking and spallation occurred in the as-sprayed coating and only a thin ceramic top coat remained. It is obvious that the spallation was initiated and propagated in the ceramic top coat close to the top coat-bond coat interface. Therefore the failure

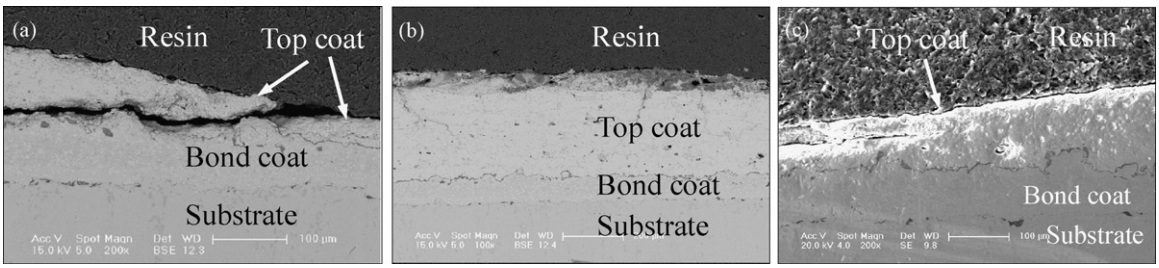

Fig. 5. Cross-sectional back-scattered electron micrographs (BSE) of the 8YSZ coatings after hot corrosion in the molten-salt mixture ($V_2O_5 + Na_2SO_4$): (a) plasma-sprayed; (b) Al_2O_3-clad; (c) $LaPO_4$-clad, perpendicular to the laser beam moving direction.

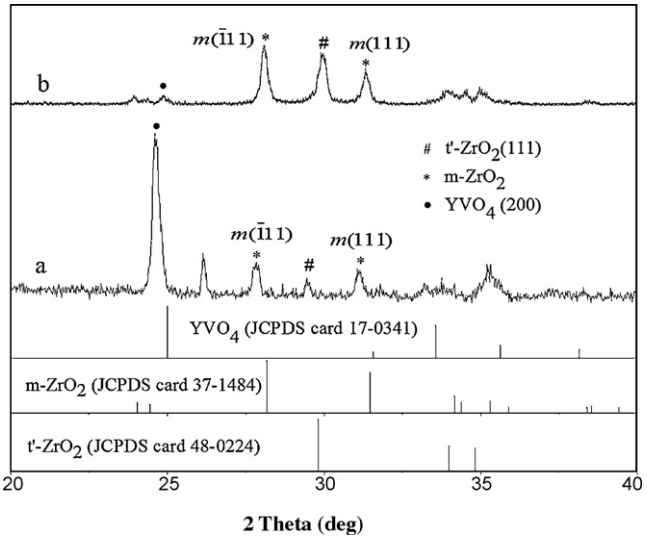

Fig. 6. XRD patterns of 8YSZ coating after hot corrosion in molten-salt mixture ($V_2O_5 + Na_2SO_4$) at 1173 K for 100 h: (a) coating surface; (b) inner area of coating.

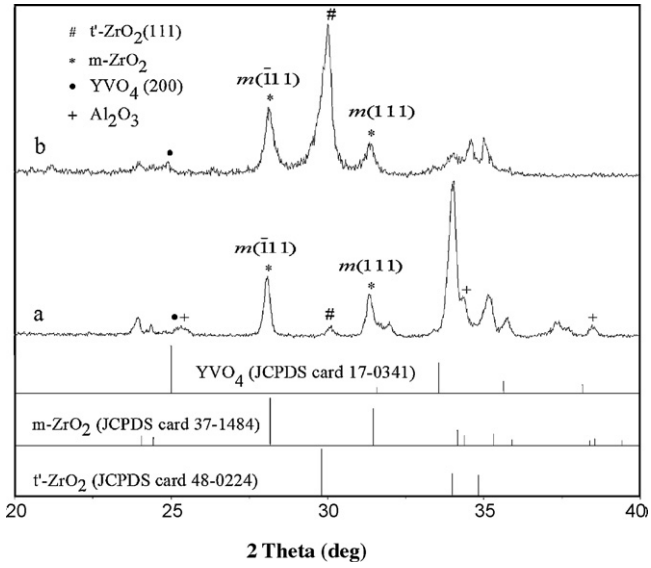

Fig. 7. XRD patterns of Al_2O_3-clad 8YSZ coating after hot corrosion in the molten-salt mixture ($V_2O_5 + Na_2SO_4$) at 1173 K for 100 h: (a) coating surface; (b) inner area of coating.

of the as-sprayed 8YSZ coating in the hot-corrosion test can be reasonably proposed to be caused predominantly by phase transformation and thermal expansion mismatch stress between the top coat and the substrate/bond coat. As can be clearly seen from Fig. 5b, the Al_2O_3-clad 8YSZ coating retains almost perfect, and neither crack nor spallation is observed. It is believed that the good hot-corrosion behavior is mainly attributed to the lower stress generated by lesser phase transformation of YSZ coating. In addition, the improvement of strain accommodation through the segmented cracks induced by laser treatment is also helpful. However, cracking and spallation are observed in the $LaPO_4$-clad 8YSZ coating after the hot-corrosion test as shown in Fig. 5c. Obviously, the spallation occurred in the ceramic top coat considerably far away from the top coat-bond coat interface, which is believed to be resulted from the serious stress induced by the significant phase transformation during the longtime test.

The XRD patterns of the exposed coatings after the hot-corrosion tests are shown in Figs. 6–8. It was found that the relative intensities of the characteristic diffraction peaks of *m*-ZrO_2 of all the exposed coatings, i.e., $m(\bar{1}\,1\,1)$ and $m(1\,1\,1)$, were significantly intensified in contrast to that before the hot-corrosion tests. The volume fractions of *m*-ZrO_2 (*%m*) within the coatings after the hot-corrosion tests are compared in Table 3, which were calculated by the peak intensity ratio formula[40]:

$$\%m = \frac{I_m(\bar{1}\,1\,1) + I_m(1\,1\,1)}{I_m(\bar{1}\,1\,1) + I_m(1\,1\,1) + I_{t'}(1\,1\,1)} \quad (1)$$

where *I* represents the diffraction intensity of the respective lattice planes.

As listed in Table 3, the volume fraction of *m*-ZrO_2 within the $LaPO_4$-clad 8YSZ coating surface is the highest among all of them. When their surfaces were ground until a layer of approximately 80 μm thick coating was removed, the volume fraction of *m*-ZrO_2 in the inner area of the as-sprayed coating was decreased to 64.8%, whereas those of the Al_2O_3-clad and $LaPO_4$-clad YSZ coatings were significantly reduced to 41.4% and 53.4%, respectively. This indicates that much lesser *t'*-ZrO_2 transformed to *m*-ZrO_2 in the inner area of the Al_2O_3-clad and $LaPO_4$-clad coatings compared to that in the as-sprayed coating after the hot-corrosion tests. In our previous work, the volume fraction of *m*-ZrO_2 in the inner area of the laser-glazed coating was decreased to 46.3% under the same conditions.[41]

The pores within the as-sprayed coating surface were mostly eliminated by laser cladding, however, to some extent, the laser-induced segmented cracks perpendicular to the coating surface served as infiltration paths for the molten salts. As proved by the XRD patterns in Figs. 6–8, YVO_4 was produced as reaction product of V_2O_5 with Y_2O_3, which consequentially caused

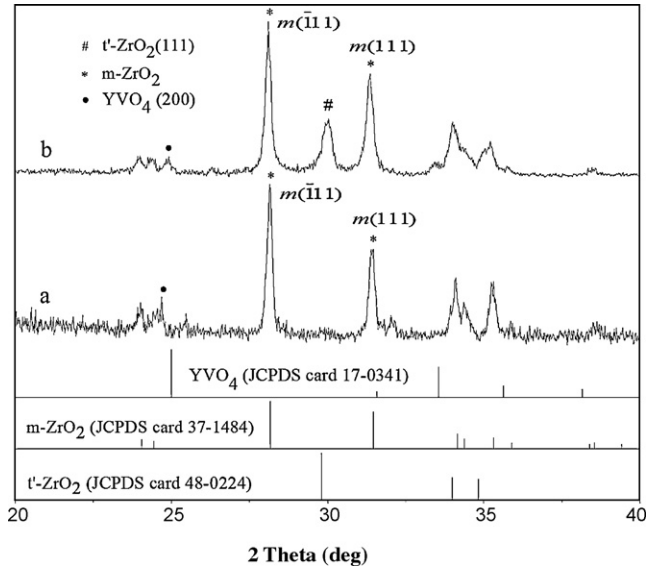

Fig. 8. XRD patterns of $LaPO_4$-clad 8YSZ coating after hot corrosion in the molten-salt mixture ($V_2O_5 + Na_2SO_4$) at 1173 K for 100 h: (a) coating surface; (b) inner area of coating.

Table 3
Volume fractions of *m*-ZrO_2 (*%m*) within the YSZ coatings after hot corrosion.

Coatings	As-sprayed		Al_2O_3-clad		$LaPO_4$-clad	
	Coating surface	[a]Inner coating	Coating surface	[a]Inner coating	Coating surface	[a]Inner coating
%m	83.5	64.8	79.2	41.4	98.6	53.4

[a] Inner coating: the surface of the coating was ground until a thin layer for approximately 80 μm was removed.

leaching of Y_2O_3 from YSZ. It is generally known that *t*′-phase of YSZ is stabilized by the presence of Y_2O_3, therefore depletion of Y_2O_3 resulted in phase transformation from *t*′- to *m*-ZrO_2. The process of *t*′- to *m*-ZrO_2 is a diffusionless, martensitic-type transformation which is accompanied by a large destructive volume expansion. The serious stresses within YSZ induced by the volume expansion can lead to cracks in the coating upon cooling and may cause coating failure further. No evidence from the XRD patterns was found that the chemical reaction between Na_2SO_4 and YSZ, Al_2O_3 or $La_7P_3O_{18}$ had taken place. This indicates that Na_2SO_4 had no chemical effect on the YSZ coating at the elevated temperature of 1173 K. A previous investigation reported that the presence of Na_2SO_4 aggravated the degradation of YSZ coating by V_2O_5 at 973 K.[42] The XRD analysis also showed that any reaction product of V_2O_5 with ZrO_2 could not be detected after the hot-corrosion tests. It is known that zirconium pyrovanadate (ZrV_2O_7) is the only compound existing in the ZrO_2–V_2O_5 system. ZrV_2O_7 melts at a temperature above 1020 K to ZrO_2 and V_2O_5,[43] and therefore no reaction product of V_2O_5 with ZrO_2 was found in this investigation. In addition, it is revealed from the XRD patterns that no reacted product of V_2O_5 with Al_2O_3 or $La_7P_3O_{18}$ is presented, which suggests that neither Al_2O_3 nor $La_7P_3O_{18}$ reacted with V_2O_5. Since the three specimens were exposed to the $V_2O_5 + Na_2SO_4$ mixture for a longtime of 100 h at 1173 K, and neither V_2O_5 nor Na_2SO_4 was presented within the coating surface based on the XRD results, probably a critical content of *m*-ZrO_2 is believed to reach for the tested coatings.

The phase transformation from *t*′- to *m*-ZrO_2 is believed to be an important factor for the failure of the as-sprayed 8YSZ coating. Those numerous pores in the as-sprayed YSZ coating provide paths for infiltration of the molten salts through the ceramic top coat, which resulted in comparatively high volume fraction of *m*-ZrO_2 in the coating after the longtime hot-corrosion test. For the Al_2O_3-clad and $LaPO_4$-clad 8YSZ coatings, the elimination of pores within the coating surfaces and the inertness between the corrosive salts and Al_2O_3 or $La_7P_3O_{18}$ effectively restrained the reaction between the corrosive salts and the inner coating, and therefore the volume fractions of *m*-ZrO_2 in the inner area of coating were significantly decreased. However, the $LaPO_4$-clad YSZ coating showed corrosion resistance inferior to the Al_2O_3-clad one. This could be attributed to the uneven-thickness clad layer that depressed the restraining effect on infiltration of the molten salts, to a certain extent.

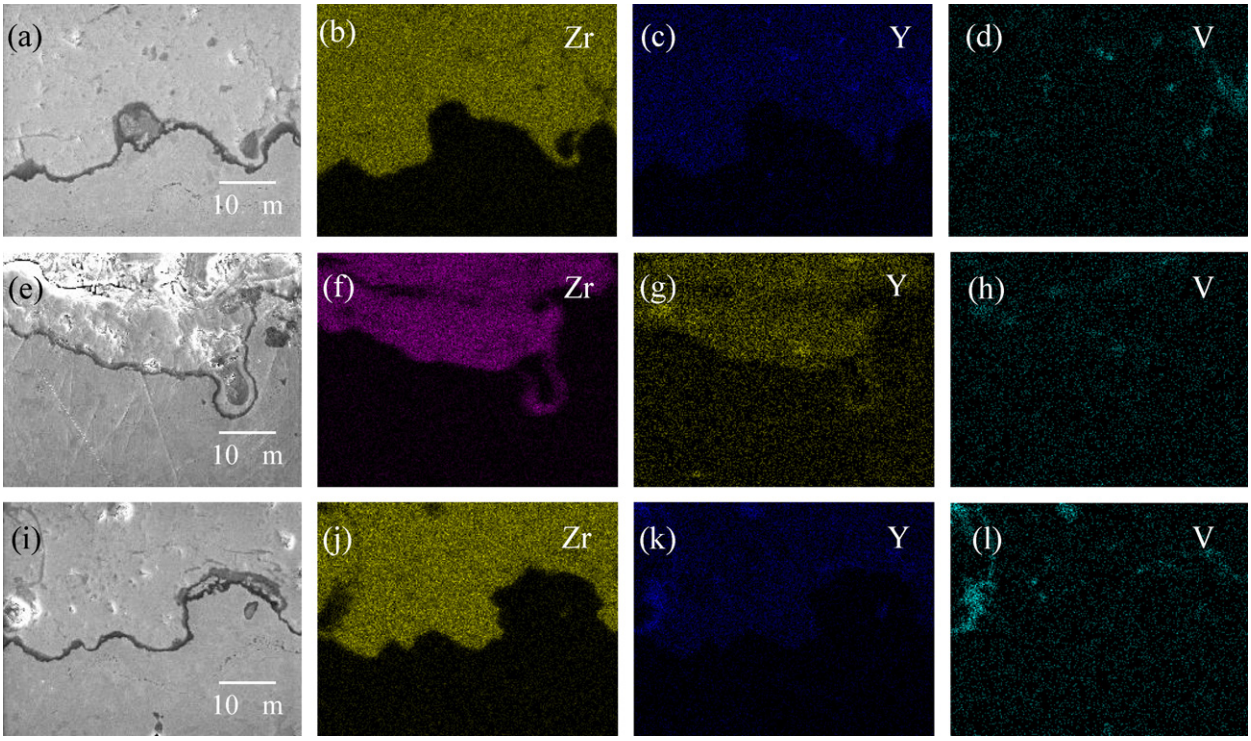

Fig. 9. High-magnification microstructures and EDS map scanning of the top coat-bond coat interface of the 8YSZ coatings after the hot-corrosion tests: (a–d) as-sprayed; (e–h) Al_2O_3-clad; (i–l) $LaPO_4$-clad.

Fig. 9 shows high-magnification microstructures and elemental distributions at the top coat-bond coat interface of the as-sprayed and overlay-clad 8YSZ coatings after the hot-corrosion tests. Neither sodium nor sulfur was detected, implying that Na_2SO_4 did not reach the top coat-bond coat interface. The molten V_2O_5 ultimately penetrated into the top coat-bond coat interface after the longtime tests as shown in Fig. 9d, h and l, even though the clad layer was presented. As shown in Fig. 9b–d, f–h, and j–l, vanadium exists in the regions which contain high quantity of yttrium and low quantity of zirconium, revealing leaching of Y_2O_3 out of 8YSZ by reaction between V_2O_5 and Y_2O_3. The distributions of vanadium in Fig. 9d and l are more intensive than that in Fig. 9h, implying that the clad Al_2O_3 layer depressed the infiltration of molten V_2O_5 through the coating more effectively.

4. Conclusion

The plasma-sprayed 8YSZ coating achieved a dense clad layer and other characteristic features of laser-treated ceramic materials. In contact with the $V_2O_5 + Na_2SO_4$ corrosive species for a longtime of 100 h at 1173 K, the Al_2O_3-clad 8YSZ coating exhibited good hot-corrosion behavior and consequently obtained a prolonged lifetime. The $LaPO_4$-clad YSZ coating exhibited corrosion resistance inferior to the Al_2O_3-clad one. The reaction between V_2O_5 and Y_2O_3 produced YVO_4, leaching Y_2O_3 from YSZ and causing the progressive destabilization transformation from t'- to m-ZrO_2. The failure of the as-sprayed coating is mainly attributed to the phase destabilization and thermal mismatch stress. The chemical inertness between V_2O_5 and α-Al_2O_3 or $La_7P_3O_{18}$, and the dense clad layers that restrained infiltration of the molten corrosive salts through the coatings led to relatively low m-ZrO_2 content in the inner area of the coatings after the hot-corrosion tests. These two factors are primary contributions to the enhancement of hot-corrosion resistances of the overlay-clad YSZ coatings. In addition, the segmented cracks in the coating surface induced by laser treatments were also helpful in improvement of thermal-shock resistance.

Acknowledgements

The authors would like to thank Dr. Yaomin Wang from Jilin Province Laser Institute, Changchun, China, for his invaluable assistance during laser cladding, Prof. Quansheng Wang of Beijing Polytechnic University for the invaluable assistance in plasma-spraying. The discussions about SEM results with Ms. Meiye Li (Changchun Institute of Applied Chemistry, China) are highly appreciated by the authors. This work was financially supported by the project of NSFC-50825204.

References

[1]. Shillington EAG, Clarke DR. Spalling failure of a thermal barrier coating associated with aluminum depletion in the bond-coat. *Acta Mater* 1999;**4**(4):1297–305.
[2]. Padture NP, Gell M, Jordan EH. Thermal barrier coatings for gas turbine engine applications. *Science* 2002;**296**:280–4.
[3]. Gleeson B. Thermal barrier coatings for aeroengine applications. *J Propul Power* 2006;**22**(2):375–83.
[4]. Evans AG, Mumm DR, Hutchinson JW, Meier GH, Pettit FS. Mechanisms controlling the durability of thermal barrier coatings. *Prog Mater Sci* 2001;**46**:505–55.
[5]. El-Turki A, Allen GC, Younes CM, Day JCC. An investigation of the effect of thermal cycling on plasma-sprayed zirconia/NiCoCrAlY thermal barrier coating. *Mater Corros* 2004;**55**(1):24–9.
[6]. Schmitt-Thomas KhG, Hertter M. Improved oxidation resistance of thermal barrier coatings. *Surf Coat Technol* 1999;**120–121**:84–8.
[7]. Jones RL. Some aspects of the hot corrosion of thermal barrier coatings. *J Therm Spray Technol* 1997;**6**(1):77–84.
[8]. Wu NQ, Chen Z, Mao SX. Hot corrosion mechanism of composite alumina/yttria-stabilized zirconia coating in molten sulfate-vanadate salt. *J Am Ceram Soc* 2005;**88**(3):675–82.
[9]. Marple BR, Voyer J, Moreau C, Nagy DR. Corrosion of thermal barrier coatings by vanadium and sulfur compounds. *Mater High Temp* 2000;**17**(3):397–412.
[10]. Gurrappa I. Hot corrosion of protective coatings. *Mater Manuf Process* 2000;**15**(5):761–73.
[11]. Marple BR, Voyer J, Thibodeau M, Vassen R. Hot corrosion of lanthanum zirconate and partially stabilized zirconia thermal barrier coatings. *J Eng Gas Turb Power* 2006;**128**:144–52.
[12]. Knuuttila J, Sorsa P, Mäntylä T. Sealing of thermal spray coatings by impregnation. *J Therm Spray Technol* 1999;**8**(2):249–57.
[13]. Ahmaniemi S, Vuoristo P, Mäntylä T. Improved sealing treatments for thick thermal barrier coatings. *Surf Coat Technol* 2002;**151–152**:412–7.
[14]. Batista C, Portinha A, Ribeiro RM, Teixeira V, Costa MF, Oliveira CR. Morphological and microstructural characterization of laser-glazed plasma-sprayed thermal barrier coatings. *Surf Coat Technol* 2006;**200**:2929–37.
[15]. Batista C, Portinha A, Ribeiro RM, Teixeira V, Costa MF, Oliveira CR. Surface laser-glazing of plasma-sprayed thermal barrier coatings. *Appl Surf Sci* 2005;**247**:313–9.
[16]. Tsai HL, Tsai PC. Performance of laser-glazed plasma-sprayed (ZrO_2–12 wt.% Y_2O_3)/Ni–22 wt.% Cr–10 wt.% Al–1 wt.%-Y thermal barrier coatings in cyclic oxidation tests. *Surf Coat Technol* 1995;**71**:53–9.
[17]. Tsai HL, Tsai PC. Thermal cyclic response of laser-glazed plasma-sprayed ZrO_2–19.5 wt%–Y_2O_3/Ni–22Cr–10Al–1Y thermal barrier coatings. *Mater Sci Eng A* 1994;**177**(1–2):227–32.
[18]. Tsai HL, Tsai PC. Microstructures and properties of laser-glazed plasma-sprayed ZrO_2–YO1.5/Ni–22Cr–10Al–1Y thermal barrier coatings. *J Mater Eng Perform* 1995;**4**(6):689–96.
[19]. Tsai PC, Hsu CS. High temperature corrosion resistance and microstructural evaluation of laser-glazed plasma-sprayed zirconia/MCrAlY thermal barrier coatings. *Surf Coat Technol* 2004;**183**(1):29–34.
[20]. Tsai PC, Lee JH, Hsu CS. Hot corrosion behavior of laser-glazed plasma-sprayed YSZ thermal barrier coatings in the presence of V_2O_5. *Surf Coat Technol* 2007;**201**:5143–7.
[21]. Petitbon A, Boquet L. Laser surface sealing and strengthening of zirconia coatings. *Surf Coat Technol* 1991;**49**:57–61.
[22]. Chwa SO, Ohmori A. Microstructures of ZrO_2–8 wt.% Y_2O_3 coatings prepared by a plasma laser hybrid spraying technique. *Surf Coat Technol* 2002;**153**:304–12.
[23]. Miller RA, Berndt CC. Performance of thermal barrier coatings in high heat flux environments. *Thin Solid Films* 1984;**119**:195–202.
[24]. Troczynski T, Yang Q, John G. Post-deposition treatment of zirconia thermal barrier coatings using sol–gel alumina. *J Therm Spray Technol* 1999;**8**(2):229–34.
[25]. Zhou M, Yang Q, Troczynski T. Effect of substrate surface modification on alumina composite sol–gel coatings. *Surf Coat Technol* 2006;**200**:2800–4.
[26]. Mäntylä T, Vuoristo P, Kettunen P. Chemical vapor deposition densification of plasma-sprayed oxide coatings. *Thin Solid Films* 1984;**118**:437–44.
[27]. Chen Z, Wu NQ, Singh J, Mao SX. Effect of Al_2O_3 overlay on hot-corrosion behavior of yttria-stabilized zirconia coating in molten sulfate–vanadate salt. *Thin Solid Films* 2003;**443**:46–52.

[28]. Afrasiabi A, Saremi M, Kobayashi A. A comparative study on hot corrosion resistance of three types of thermal barrier coatings: YSZ, YSZ + Al_2O_3 and YSZ/Al_2O_3. *Mater Sci Eng A* 2008;**478**:264–9.

[29]. Ramachandra C, Lee KN, Tewari SN. Durability of TBCs with a surface environmental barrier layer under thermal cycling in air and in molten salt. *Surf Coat Technol* 2003;**172**:150–7.

[30]. Wu NQ, Chen Z, Mao SX. Hot corrosion mechanism of composite alumina/yttria-stabilized zirconia coating in molten sulfate–vanadate salt. *J Am Ceram Soc* 2005;**88**(3):675–82.

[31]. Yue TM, Huang KJ, Man HC. In-situ laser cladding of Al_2O_3 reaction coating on aluminum alloy 7075 for corrosion resistance improvement. *Mater Trans* 2006;**47**:948–51.

[32]. Ouyang JH, Nowotny S, Richter A, Beyer E. Characterization of laser clad yttria partially-stabilized ZrO_2 ceramic coatings on steel $16MnCr_5$. *Surf Coat Technol* 2001;**137**:12–20.

[33]. Yue M, Duan ZP, Yang ZX, Wu CK. Application of laser cladding technology to improve the interface of thermal barrier coatings. *Surf Interface Anal* 2000;**29**:310–3.

[34]. Sudre O, Cheung J, Marshall D, Morgan P, Levi CG. Thermal insulation coatings of $LaPO_4$. In: Singh M, Jessen T, editors. *The 25th Annual International Conference on Composites, Advanced Ceramics, Materials, and Structures: B*. Westerville, OH, USA: American Ceramic Society; 2001. p. 367–74.

[35]. Morgan PED, Marshall DB. Ceramic composites of monazite and alumina. *J Am Ceram Soc* 1995;**78**(6):1553–63.

[36]. Krishnan R, Dash S, Babu Rao C, Subba Rao RV, Tyagi AK, Baldev Raj. Laser induced structural and microstructural transformations of plasma sprayed Al_2O_3 coatings. *Scripta Mater* 2001;**45**:693–700.

[37]. Krishnan R, Dash S, Sole RK, Tyagi AK, Baldev Raj. Fabrication and characterisation of laser surface modified plasma sprayed alumina coatings. *Surf Eng* 2002;**18**(3):208–12.

[38]. Wang D, Tian Z, Shen L, Liu Z, Huang Y. Influences of laser remelting on microstructure of nanostructured Al_2O_3–13 wt.% TiO_2 coatings fabricated by plasma spraying. *Appl Surf Sci* 2009;**255**:4606–10.

[39]. Krishnan R, Kesavamoorthy R, Dash S, Tyagi AK, Baldev Raj. Raman spectroscopic and photoluminescence investigations on laser surface modified α-Al_2O_3 coatings. *Scripta Mater* 2003;**48**:1099–104.

[40]. Brandon JR, Taylor R. Phase stability of zirconia-based thermal barrier coatings. Part I: zirconia–yttria alloys. *Surf Coat Technol* 1991;**46**: 75–90.

[41]. Zhong, X., Wang, Y., Xu, Z., Zhang, Y., Zhang, J. and Cao, X., Influence of laser-glazing on hot-corrosion resistance of yttria-stabilized zirconia TBC in molten salt mixture of V_2O_5 and Na_2SO_4. *Mater. Corros.*, doi:10.1002/maco.200905209.

[42]. Mohan P, Yuan B, Patterson T, Desai VH, Sohn YH. Degradation of yttria-stabilized zirconia thermal barrier coatings by vanadium pentoxide, phosphorous pentoxide, and sodium sulfate. *J Am Ceram Soc* 2007;**90**:3601–7.

[43]. Buchanan RC, Wolter GW. Properties of hot-pressed zirconium pyrovanadate ceramics. *J Electrochem Soc* 1983;**130**(9):1905–10.